

# Artificial gravitation effect on spin-polarized exciton-polaritons

E. S. Sedov<sup>1,2,\*</sup> and A. V. Kavokin<sup>1,3,4,†</sup>

<sup>1</sup>*School of Physics and Astronomy, University of Southampton, SO17 1NJ Southampton, United Kingdom*

<sup>2</sup>*Department of Physics and Applied Mathematics,*

*Vladimir State University named after A. G. and N. G. Stoletovs, Gorky str. 87, 600000, Vladimir, Russia*

<sup>3</sup>*CNR-SPIN, Viale del Politecnico 1, I-00133, Rome, Italy*

<sup>4</sup>*Spin Optics Laboratory, St. Petersburg State University,  
Ul'anovskaya 1, Peterhof, St. Petersburg 198504, Russia*

The pseudospin dynamics of long-living exciton-polaritons in a wedged 2D cavity has been studied theoretically accounting for the external magnetic field effect. The cavity width variation plays the role of the artificial gravitational force acting on a massive particle: exciton-polariton. A semi-classical model of the spin-polarization dynamics of ballistically propagating exciton-polaritons has been developed. It has been shown that for the specific choice of the magnetic field magnitude and the initial polariton wave vector the polariton polarization vector tends to an attractor on the Poincaré sphere. Based on this effect, the switching the polariton polarization in the ballistic regime has been demonstrated. The self-interference of the polariton field emitted by a point-like source has been shown to induce the formation of interference patterns reminiscent of the interference patterns of cylindrical and plane waves.

---

\* Electronic address: [evgeny\\_sedov@mail.ru](mailto:evgeny_sedov@mail.ru)

† Electronic address: [a.kavokin@soton.ac.uk](mailto:a.kavokin@soton.ac.uk)

## I. INTRODUCTION

Exciton-polaritons in 2D semiconductor cavity structures being an equipollent combination of cavity photons and elementary matter excitations (excitons) and exhibiting properties of both their constituents represent a fascinating object for study both from the fundamental point of view and for applications in opto-electronics. Until recently, one of the key constraints for observation of long-range polariton propagation was the extremely short polariton lifetime which in the best case wouldn't exceed few tens of picoseconds [1, 2]. Since exciton-polaritons are composite quasiparticles arising due to the strong coupling of photons and excitons, they have a finite lifetime that is governed by lifetime of photons in the cavity [3]. In recent papers [4, 5] an increase of the polariton lifetime up to of the order of 100 ps due to the use of specially designed 2D cavities with ultra-high quality factors has been reported. In these structures, polaritons can move away from the excitation spot by the distances of the order of a few millimetres in a cavity plane. The possibility of generation of a long-range coherent polariton flow in high-finesse microcavities is very promising for realization of ultrafast optoelectronic devices.

Given the possibility of long-living polaritons excitation, a subject of the control of their spatial dynamics arises. One of the convenient approaches to manipulation of exciton-polariton dynamical characteristics is through the generation of an external potential of a required configuration. In this context, the idea of polariton acceleration in a cavity with the gradient of the cavity thickness has been discussed in [6] and then developed in [7]. Reduction of the cavity width leads to a positive shift of the lower dispersion branch (LB) of polaritons. Since the latter is concave, to conserve the energy fixed, LB polaritons are forced to reduce their wave vector component in the propagation direction. Their group velocity in the same direction decreases as a result. As it has been shown in [7], in samples where the cavity width decreases linearly with one of the in-plane coordinates polaritons propagate on parabolic trajectories. Herewith, contribution of a cavity thickness variation can be described as an effect of an external constant force analogous to the gravitational force acting on massive particles.

Due to the specificity of the polariton dynamics in such conditions, polaritons have been observed to slow down until a complete stop and then reverse their propagation direction [7]. The authors of Ref. 7 refer to such type of motion as “slow reflection”. This effect has been proposed in [8] as a tool for suppression of the light reflection by the edge of the sample which is essential for diminishing the parasitic effects caused by interference polaritons propagating towards the edge with the reflected ones. In contrast with the normal reflection, in the case of “slow reflection” the phase of propagating polaritons does not change abruptly at the turning point but varies continuously. The latter point is essential for understanding of the non-trivial interference of the direct and reflected polariton waves, as we show below.

Exciton-polaritons are widely discussed as potential candidates for all-optical information transport, storage and processing because of their non-trivial polarization properties. The cavity polariton polarization is mostly dependent on two factors that are the long-range electron-hole exchange interaction [9] and the polarization splitting of the photonic cavity modes [10]. In particular, the TE-TM splitting of the cavity eigenmodes leads to the splitting of linearly polarized polariton dispersion branches that induces the precession of the polarization vector of propagating polaritons [11, 12]. One can describe the polariton polarization using the pseudospin formalism [13–15]. The polariton TE-EM splitting effect can be described as the polariton pseudospin precession around an effective magnetic field applied in the cavity plane. The non-trivial polariton pseudospin dynamics has been revealed in a wide range of experimentally observed effects including the polarization multistability [16], spin switching [17], optical spin Hall effect [14], etc. In the presence of the external magnetic field  $\mathbf{B}$ , the polariton pseudospin dynamics becomes even more complicated. For the field applied in the Faraday geometry ( $\mathbf{B}$  is normal to the cavity plane and is collinear with the incident light wave vector), the exciton-polariton energy band structure is enriched with the Zeeman splitting of right- and left-circularly polarized polariton states [18, 19].

In this paper, we consider the pseudospin dynamics of long-living polaritons in a wedged 2D microcavity under the influence of the “gravitational” force produced by the cavity width gradient in the presence of the external magnetic field applied normally to the cavity plane. The paper is organized as following. In Sec. II, we discuss the model describing the polariton polarization dynamics within the pseudospin formalism. Section III presents the study of a particular case of polariton propagation in the gradient direction. Section IV is devoted to a general case of the polariton propagation oblique to the effective “gravitational” field. In conclusion, we address the importance of polariton self-interference and polarization effects in the “slow reflection” regime.

## II. BALLISTIC MOTION OF EXCITON-POLARITONS IN GRADED MICROCAVITIES

The considered geometry of the problem is schematically shown in Fig. 1. It basically coincides with that studied experimentally in Refs. 4 and 7. The sample represents a semiconductor microcavity with embedded quantum wells that are holders of excitons. The cavity is characterized by a linear variation of the thickness in  $y$ -direction that causes

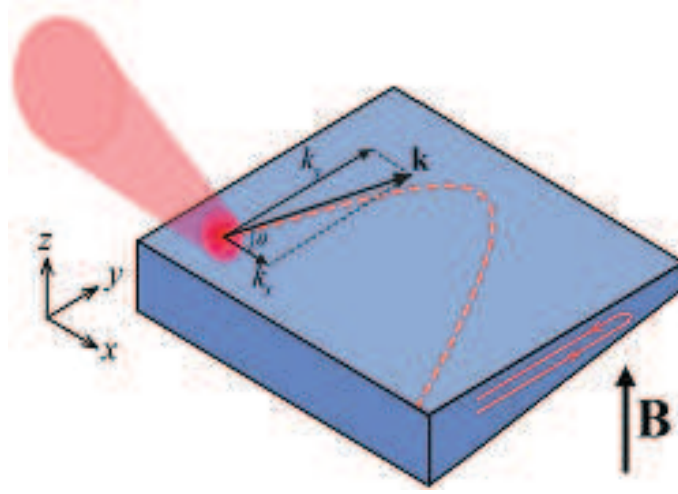


FIG. 1. (Color online) The schematic of the considered problem. The sample represents a 2D electrodynamic microcavity with embedded ensemble of semiconductor quantum wells. The width of the cavity in  $z$  direction gradually decreases along  $y$  axis. Polaritons are injected in the sample by a laser beam inclined to the cavity plane. By manipulation the angle of inclination, one possible to control the polariton kinetic energy in the sample in  $xy$  plane. An external magnetic field  $\mathbf{B}$  is applied to the system normally to the cavity plane.

a polariton energy gradient in the same direction. The exciton-polaritons are supposed to be excited resonantly by the external laser beam. We shall consider both the regime of excitation by ultrashort laser pulses and the regime of continuous wave pumping. The initial quantum state of generated polaritons, their polarization, energy and wave vector are supposed to be set by the exciting laser.

One can fully characterize the polarization (pseudospin) state of cavity polaritons by the four-component Stokes vector  $(S_0, S_x, S_y, S_z)$ , where  $S_{x,y,z}$  characterize the intensities of linear (collinear with the original coordinate basis axes components and diagonal/antidiagonal ones) and circular polarization components, respectively, while  $S_0 = \sqrt{S_x^2 + S_y^2 + S_z^2}$  corresponds to the total intensity of a polarized polariton wave [13]. For the completely polarized wave  $S_0$  remains unchanged during the polariton propagation. Using this fact, for further calculations we introduce the three-component vector  $\mathbf{S} = (S_x, S_y, S_z)$  with  $S_{x,y,z}$  being given in units of  $S_0$ ;  $|S_{x,y,z}| \leq 1$ .

In the presence of the effective magnetic field, the dynamics of Stokes vector components is described by the following equation [14]:

$$\frac{d\mathbf{S}}{dt} = \mathbf{\Omega} \times \mathbf{S}, \quad (1)$$

where the effective magnetic field  $\mathbf{\Omega}$  (gauge field) components are

$$\Omega_x = \frac{\Delta_{LT} (k_x^2 - k_y^2)}{\hbar (k_x^2 + k_y^2)}, \quad \Omega_y = \frac{2\Delta_{LT} k_x k_y}{\hbar (k_x^2 + k_y^2)} \quad (2)$$

with the TE-TM splitting given by

$$\Delta_{LT} = \frac{\hbar^2}{2M} (k_x^2 + k_y^2). \quad (3)$$

In (3)  $M = \frac{m_{TE}^* m_{TM}^*}{m_{TE}^* - m_{TM}^*}$  and  $m_{TE}^*$ ,  $m_{TM}^*$  are the effective masses of TE- and TM-polarized polariton field components.  $k_{x,y}$  are Cartesian components of the polariton wave vector  $\mathbf{k}$ .

In the simplest model case, the dynamics of a single polariton as well as one of a polariton wave packet can be characterized by particle-like dynamics of its “center of gravity” having the coordinates  $(x_0, y_0)$  that change in time,  $x_0 \equiv x_0(t)$  and  $y_0 \equiv y_0(t)$ . The classical mechanical approach yields the following equations for the particle trajectories:

$$x_0(t) = \frac{\hbar k_x}{m^*} t, \quad (4a)$$

$$y_0(t) = \frac{\hbar k_{y,0}}{m^*} t - \frac{\beta}{2m^*} t^2, \quad (4b)$$

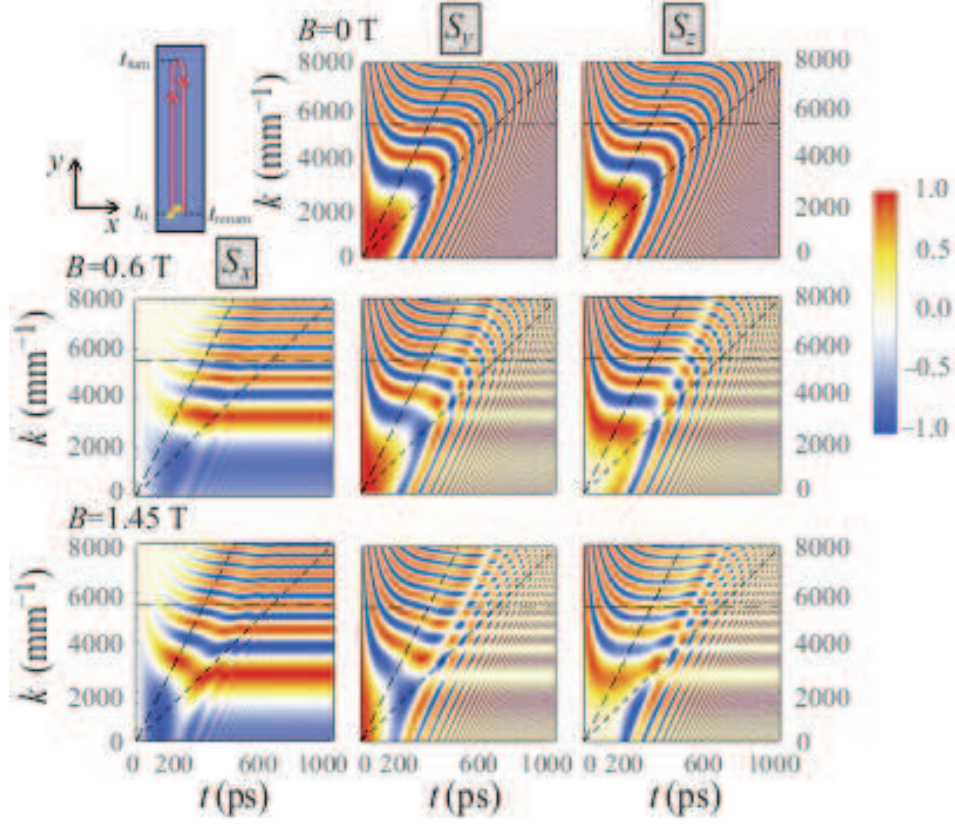


FIG. 2. (Color online) The dynamics of the polariton polarization components  $S_{x,y,z}$  (from the left panels to the right panels) in the case of polariton propagation along the gradient of the thickness as a function of the initial wave number  $k_0$  for  $B = 0$  T (the upper panels), 0.6 T (the middle panels) and 1.45 T (the lower panels). The left upper panel shows schematically the polariton trajectory. The initial polarization is taken diagonal linear with the initial conditions  $S_{y,0} = 1$ ,  $S_{x,z,0} = 0$ . The parameters used for this calculation are given in the text of the paper.

where  $m^* = \frac{m_{TE}^* m_{TM}^*}{m_{TE}^* + m_{TM}^*}$  is the effective mass of the particle;  $k_{y,0} \equiv k_y(t = 0)$  is the corresponding wave vector component at the starting time moment. The impact of the “gravitational” force  $F = -\beta$  caused by the sample thickness gradient is taken into account by introducing the linear variation of the polariton potential energy in  $y$ -direction.

In the considered geometry, the wave vector  $\mathbf{k}$  is time-dependent as well. The dependence  $k_y(t)$  can be derived from the energy conservation condition:

$$\beta y_0 + \frac{\hbar^2 (k_x^2 + k_y^2)}{2m^*} = E_0, \quad (5)$$

where the first term in the left hand side of the equation is the potential energy and the second term is the kinetic energy. The total energy  $E_0$  appearing in the right hand side is equal to the kinetic energy at  $t = 0$  and it is set by the exciting laser beam properties. Hence

$$k_y = \pm \sqrt{\frac{2m^*}{\hbar^2} \left( E_0 - \beta y_0 - \frac{\hbar^2 k_x^2}{2m^*} \right)}, \quad (6)$$

where “+” corresponds to the propagation of polaritons before the turning point (in the direction of the cavity thickness gradient) while “−” describes the propagation after the turning point (in the opposite direction).  $k_x$  remains constant during the polariton propagation.

In the absence of external magnetic fields,  $\Omega_z = 0$ . Switching on of the magnetic field  $\mathbf{B}$  in normal to the cavity plane direction ( $B_{x,y} = 0$ ) removes the degeneracy in  $z$  direction that leads to the appearance of the third component of the vector  $\boldsymbol{\Omega}$ :

$$\Omega_z = \frac{\mu_B g B}{\hbar}, \quad (7)$$

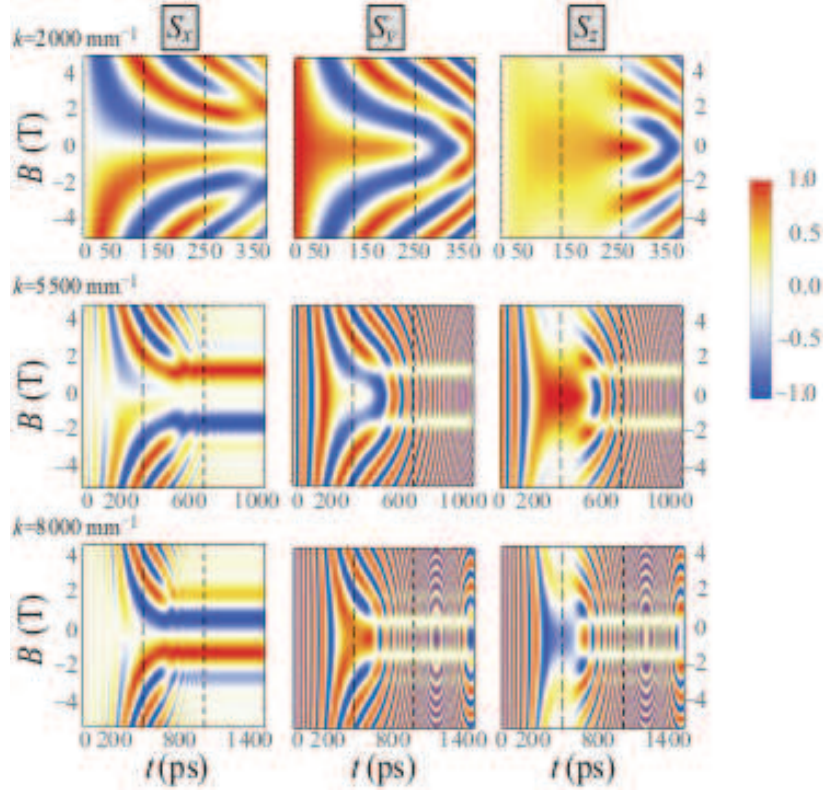


FIG. 3. (Color online) The dynamics of the polariton polarization components  $S_{x,y,z}$  (from the left panels to the right panels) in the case of polariton propagation along the gradient of the thickness as a function of the magnetic field  $B$  for  $k = 2000 \text{ mm}^{-1}$  (the upper panels),  $5500 \text{ mm}^{-1}$  (the middle panels) and  $8000 \text{ mm}^{-1}$  (the lower panels). The initial conditions and the parameters are taken the same as in Fig. 2.

where  $\mu_B$  is the Bohr magneton,  $g$  is the polariton g-factor and  $B \equiv |\mathbf{B}|$ .

It is important to underline that in contrast with the problem considered in Ref. 14, the absolute value and the orientation of the vector  $\mathbf{\Omega}$  acting on a specific ballistically propagating polariton becomes time- and coordinate-dependent due to the “effective gravity”. The polarization components oscillate with a frequency  $\Omega = \sqrt{\Omega_x^2 + \Omega_y^2 + \Omega_z^2}$  that is changing with the particle propagation.

Below we list the parameters used for the numerical modelling. Following [7], we consider polaritons possessing the effective mass of  $m^* = 5 \times 10^{-5} m_e$  with  $m_e$  being the vacuum electron mass;  $m_{\text{TE}}^* \simeq 9.068 \times 10^{-35} \text{ kg}$  and  $m_{\text{TM}}^* \simeq 9.132 \times 10^{-35} \text{ kg}$ . We consider a sample which provides the “gravitational” force  $F = -10.5 \text{ meV/mm}$ . Polariton g-factor is  $g = 0.1$ . The initial wave number  $k$  and the initial kinetic energy  $E_0$  can be tuned by changing the angle of incidence of the pump.

### III. POLARITON PROPAGATION IN THE DIRECTION OF THE THICKNESS GRADIENT

#### A. Single Polariton Propagation

Let us first consider polaritons propagating in the “gravitation” force vector direction ( $y$ -direction). To control the polarization state of polaritons, we have three external parameters. The first one is the “gravitational” force strength governed by the parameter  $\beta$ . In the absence of external magnetic fields ( $B = 0$ ) the “gravitational” force doesn’t affect  $k_x$  component of the wave vector thus it remains unchanged during the polariton propagation. In the considered case  $k_x = 0$ , according to Eq. (2) we have  $\Omega_y = 0$  and  $\Omega_z = 0$  as well, so that, Eq. (1) yields  $dS_x/dt = 0$ . Thus for the initial conditions  $S_{y,0} = S_{z,0} = 0$  and  $S_{x,0} = \pm 1$  the linear polarization is conserved in the course of the polariton propagation and the Stokes vector points to  $(\pm 1, 0, 0)$  on the Poincaré sphere.

For the initial conditions  $S_{y,0} \neq 0$  or/and  $S_{z,0} \neq 0$  and  $|S_{x,0}| < 1$  the parameter  $S_x$  remains constant while  $S_{y,z}$



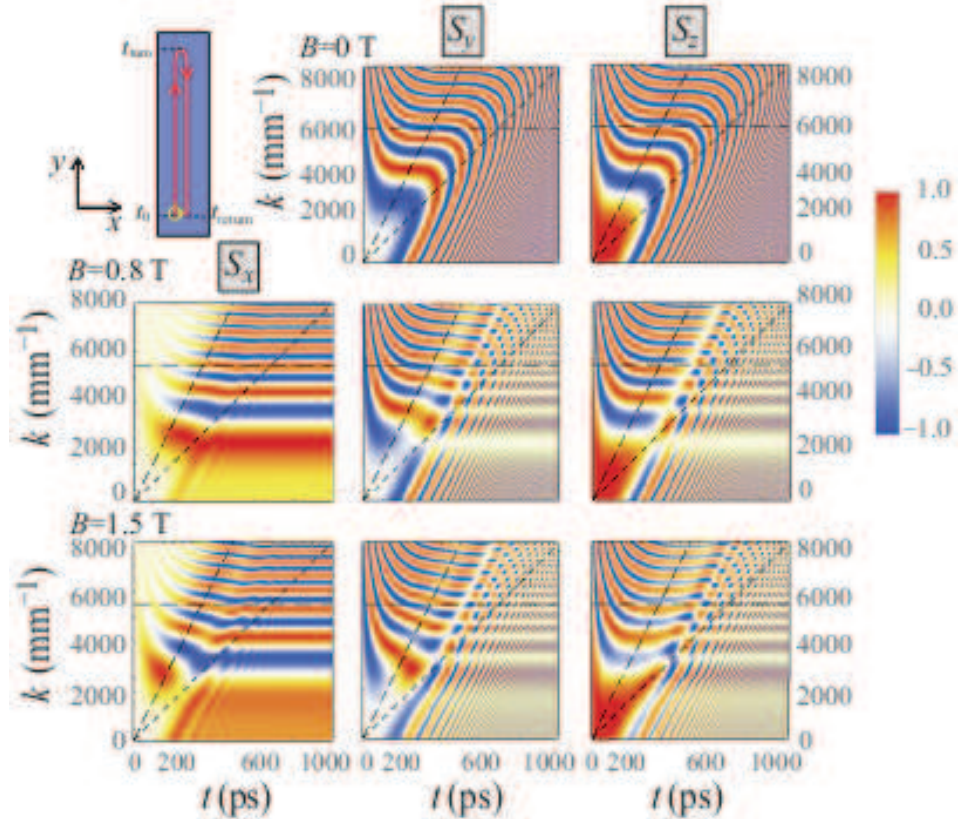


FIG. 4. (Color online) The dynamics of the polariton polarization components  $S_{x,y,z}$  (from the left panels to the right panels) in the case of polariton propagation along the gradient of the thickness as a function of the initial wave number  $k$  for  $B = 0$  T (the upper panels), 0.8 T (the middle panels) and 1.5 T (the lower panels). The left upper panel shows schematically the polariton trajectory. The initial polarization is taken circular with the initial conditions  $S_{z,0} = 1$ ,  $S_{x,y,0} = 0$ . The parameters used for this calculation are the same as in Figs. 2, 3.

components oscillate in the range  $(-\sqrt{1 - S_{x,0}^2}, \sqrt{1 - S_{x,0}^2})$ . The solution of Eq. (1) can be easily found analytically in the form

$$S_x = S_{x,0}, \quad (8a)$$

$$S_y = S_{y,0} \cos[f(t)] + S_{z,0} \sin[f(t)], \quad (8b)$$

$$S_z = S_{z,0} \cos[f(t)] - S_{y,0} \sin[f(t)], \quad (8c)$$

where  $f(t) = \frac{t}{\hbar M} \left[ E_0 m^* - \frac{\hbar}{2} \beta k_{y,0} t + \frac{\beta^2 t^2}{6} \right]$ . The energy transfer between the circular and the diagonal linear polarization modes is clearly seen. The polariton Stokes vector describes a circular trajectory on the Poincaré sphere at  $S_x = S_{x,0}$  in this case.

Another polarization dynamics control parameter is the initial wave vector  $\mathbf{k}$  in the  $xy$  plane. Slightly changing the value of  $k = |\mathbf{k}|$  one can enhance or diminish the impact of the “gravitational” force on the dynamics of the polarization components.

The third control parameter is an external magnetic field perpendicular to the cavity plane. It makes  $S_x$  time-dependent and allows for manipulating the output polarization when keeping  $k$  unchanged.

The color maps in Figs. 2 and 3 illustrate the dynamics of the polariton polarization components  $S_{x,y,z}$  as functions of the initial wave number  $k$  for a number of values of the external magnetic field magnitude  $B$  (Fig. 2) and on the value of  $B$  for different  $k$  (Fig. 3). Similar color maps are presented in Figs. 4 and 5 for the initial circular polarization with  $S_{z,0} = 1$ ,  $S_{x,y,0} = 0$ . The inclined broad-dashed (left) lines in Figs. 2 and 4 indicate the turning times,  $t_{\text{turn}}$ , when polaritons reach the furthest point in  $y$  direction for the given initial  $k$ . At this moment  $k_y(t_{\text{turn}}) = 0$ . The inclined narrow-dashed (right) lines indicate the time  $t_{\text{return}}$  when polaritons return to the starting point  $(x_0(t_{\text{out}}), y_0(t_{\text{out}})) = (0, 0)$ . The horizontal dash-dotted lines label the polarization state dynamics at  $k = 5.5 \times 10^3 \text{ mm}^{-1}$ . The vertical dashed lines in Figs. 3 and 5 correspond to  $t_{\text{turn}}$  (left) and  $t_{\text{return}}$  (right).

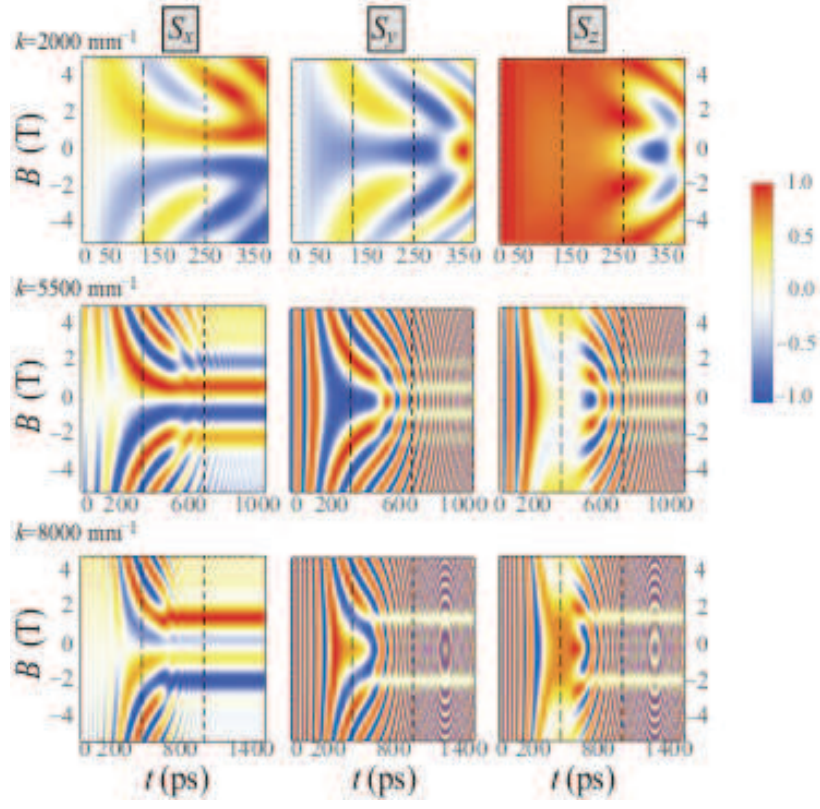


FIG. 5. (Color online) The dynamics of the polariton polarization components  $S_{x,y,z}$  (from the left panels to the right panels) in the case of polariton propagation along the gradient of the thickness as a function of the magnetic field  $B$  for  $k = 2000 \text{ mm}^{-1}$  (the upper panels),  $5500 \text{ mm}^{-1}$  (the middle panels) and  $8000 \text{ mm}^{-1}$  (the lower panels). The initial conditions and the parameters are taken the same as in Fig. 4.

Let us now consider in detail the main peculiarities of the polariton polarization dynamics illustrated by Figs. 2–5. First, the central colorless horizontal stripe in the left panels in Figs. 3 and 5 corresponding to  $B \approx 0$  confirms that  $S_x$  remains unchanged during the propagation in the absence of an external applied magnetic field.

Second, for the strong enough magnetic field,  $B \gg 1 \text{ T}$  where  $\Omega_z$  sufficiently exceeds  $\Omega_{x,y}$ , the oscillation frequency  $\Omega$  tends to a constant value,  $\Omega \rightarrow \Omega_z = \text{const}$ . For the cases of both linear and circular initial polarizations and a large magnetic field,  $S_x$  polarization component decreases at long times, see the left middle and lower panels in Figs. 3 and 5. This can be understood in terms of the interplay between the dynamics of the effective magnetic field and the dynamics of the polariton Stokes vector that precesses around this field.

Even stronger the interplay dynamical effects manifest themselves in the intermediate regime of  $\Omega_z \sim \Omega_{x,y}$ . This regime is characterized by the enhancement of the  $S_x$  component of the Stokes vector accompanied by suppression of the other components,  $S_y$  and  $S_z$ . The latter is visualised as pale stripes in the middle and right panels in Figs. 3 and 5. Herewith, for the given  $B$ , there is a discrete spectrum of  $k$  that corresponds to the appearance of such stripes. The value of  $k$  increases with the increase of the index of the stripe  $n$  approximately quadratically  $k_n^2 \propto n$ . Having in mind that  $\Omega_x \propto k^2$ , this is a signature of a resonant parametric character of the formation of closed trajectories at the surface of the Poincaré sphere as will be discussed below.

To analyse principal peculiarities of the discovered non-trivial polarization dynamics, let us track the corresponding phase trajectories on the Poincaré sphere. Examples of the resulting trajectories are shown in Fig. 6 for the linear ( $S_{y,0} = 1$ , upper panels) and circular ( $S_{z,0} = 1$ , lower panels) initial polarizations. The considered states are characterized by low-amplitude oscillations  $s_{x,y,z}(t)$  of the polarization parameters at  $t \rightarrow \infty$  around some stationary point (attractor) with  $S_x(\infty)$  different from zero. We represent the Stokes parameters as  $S_{x,y,z}(t) = S_{x,y,z}^{\text{mean}}(t) + s_{x,y,z}(t)$ , where  $S_{x,y,z}^{\text{mean}}(t)$  characterize slowly changing mean values,  $|S_{x,y,z}^{\text{mean}}| \gg |s_{x,y,z}|$  and  $dS_{x,y,z}^{\text{mean}}/dt \ll ds_{x,y,z}/dt$ . Substituting these expansions in (1), we finally obtain that  $S_y^{\text{mean}} = 0$  while the rest parameters are related between themselves as  $S_z^{\text{mean}} = \frac{\Omega_x}{\Omega_z} S_x^{\text{mean}}$ . Since  $\Omega_x$  grows with time as  $t^2$  while  $\Omega_z$  remains constant, for large enough time  $S_z^{\text{mean}}$  tends to 0. Whereas the parameters  $S_{x,y,z}$  are linked with each other through  $S_0$ , the  $S_x^{\text{mean}}$  polarization component tends to 1 for  $t \rightarrow \infty$ . Consequently, the discovered closed trajectories on the Poincaré sphere correspond to the oscillations of the

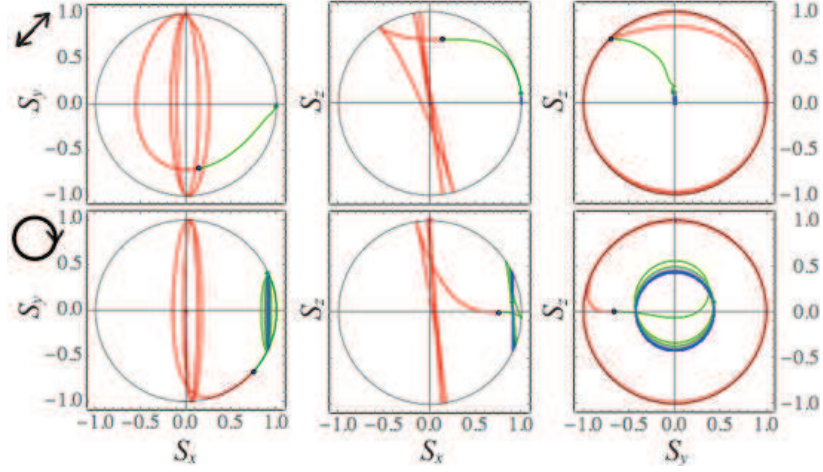


FIG. 6. (Color online) Projections of the Poincaré sphere and the trajectories of the polariton Stokes vector. In the upper panels  $B = 1.45$  T and the initial polarization is taken diagonal linear with the initial conditions  $S_{y,0} = 1$ ,  $S_{x,z,0} = 0$ . In the lower panels  $B = 0.8$  T and the initial polarization is taken circular with the initial conditions  $S_{z,0} = 1$ ,  $S_{x,y,0} = 0$ . The red-colored curves show the Stokes vector trajectories from  $t = 0$  to  $t_{\text{turn}}$ . The green- and blue-colored curves show the trajectories in the time ranges  $(t_{\text{turn}}, t_{\text{return}})$  and  $(t_{\text{return}}, 3t_{\text{return}})$ , respectively.

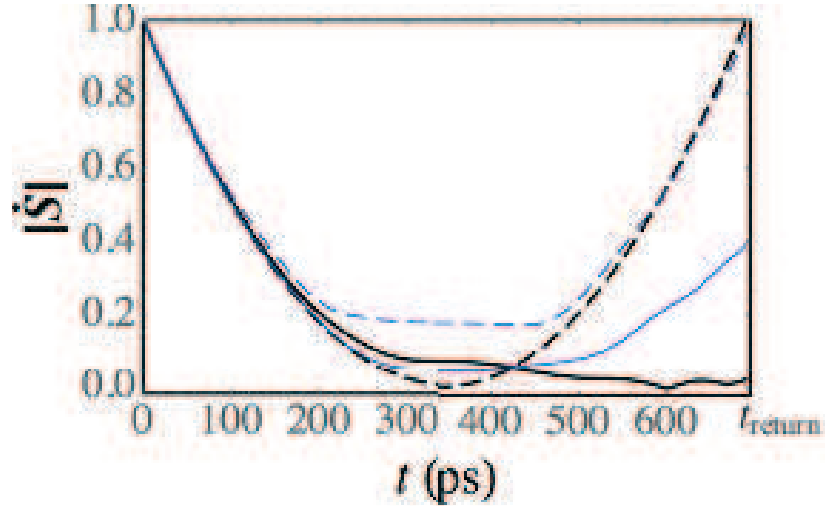


FIG. 7. (Color online) The absolute value of the time derivative of the polariton Stokes vector calculated as a function of time. The dependence is shown in the interval  $0 \leq t \leq t_{\text{return}}$ . The value of  $\dot{\mathbf{S}}(t)$  is normalized to  $\dot{\mathbf{S}}(0)$ . The bold black curves correspond to the diagonal linear initial polarization with  $S_{y,0} = 1$  while the thin blue curves correspond to the circular initial polarization with  $S_{z,0} = 1$ . The initial wave number is taken  $k = 5.5 \times 10^3 \text{ mm}^{-1}$ . The values of  $B$  are taken 0.4 T (black dashed curve), 1.45 T (black solid), 0.8 T (blue solid) and 2.5 T (blue dashed).

Stokes vector in the  $S_y S_z$  plane around the point  $(S_x^{\text{mean}} = 1, S_y^{\text{mean}} = 0, S_z^{\text{mean}} = 0)$ , see Fig. 6. Thereby, applying the external magnetic field of a specific magnitude for a given incidence angle, one can achieve switching from the diagonal linear polarization state ( $S_y = \pm 1$ ) or the circular polarization state ( $S_z = \pm 1$ ) to the linear polarization state ( $S_x \simeq \pm 1$ ).

Let us consider the behavior of the absolute value of the vector  $\dot{\mathbf{S}} = \mathbf{\Omega} \times \mathbf{S}$  given by Eq. (1). This vector characterizes precession of the polariton Stokes vector around the effective magnetic field  $\mathbf{\Omega} = (\Omega_x, \Omega_y, \Omega_z)$ . For the considered case where  $\Omega_y = 0$ , Eq. (1) yields

$$|\dot{\mathbf{S}}|^2 = \Omega_x^2 (S_y^2 + S_z^2) + \Omega_z^2 (S_x^2 + S_y^2) - 2\Omega_x \Omega_z S_x S_z. \quad (9)$$

The temporal behavior of  $|\dot{\mathbf{S}}|$  is illustrated in Fig. 7 for a number of particular cases. It is clearly seen that for the parameters corresponding to the pronounced polarization switch trajectories in Fig. 6 there is a significant reduction



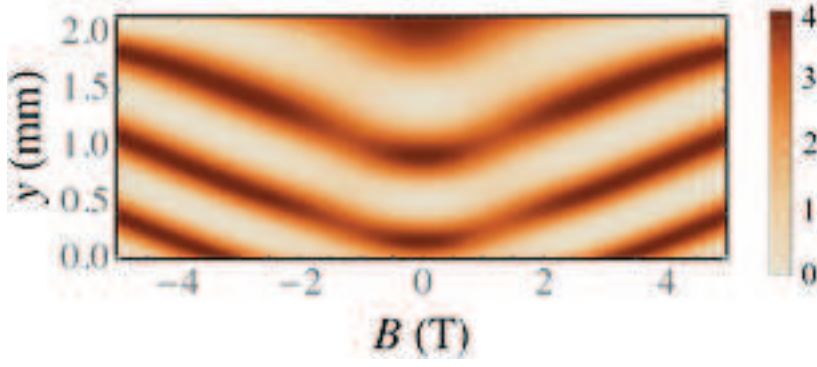


FIG. 8. (Color online) Patterns resulting from the self-interference of the polariton wave propagating along the  $y$  axis as a function of the magnitude of the external magnetic field  $B$ .

of  $|\dot{\mathbf{S}}|$  (solid lines in Fig. 7) at the times around  $t_{\text{return}}$ . The limiting case where  $|\dot{\mathbf{S}}|$  tends to zero at large time can be found if the condition is fulfilled:

$$\frac{1}{M} \left( \beta k_{y,0} - \frac{\beta^2}{\hbar} t \right) (1 - S_x) = -\frac{1}{2} \Omega_z \Omega_x S_y. \quad (10)$$

In this case, the trajectories degenerate to the point. The closest to this regime trajectories are shown in the upper panels of Fig. 6 while the corresponding dynamics of  $|\dot{\mathbf{S}}|$  is shown in Fig. 7 (bold black solid curve). The exact solutions of Eq. (10) are inachievable as  $S_{x,y}$  change with time. Nevertheless, if Eq. (10) is satisfied even approximately for  $t \sim t_{\text{return}}$ , the closed trajectories (attractors) may be seen on the surface of the Poincaré sphere.  $|\dot{\mathbf{S}}|$  slowly increases with time at  $t \rightarrow t_{\text{return}}$  in this regime.

### B. Self-Interference of Polarized Polariton Waves

Let us now consider the different excitation regime, namely the resonant cw excitation of polaritons in the spot characterized by  $x_0(0) = y_0(0) = 0$  and  $k_x = 0$ ,  $k_{y,0} = k$ . Obviously, in this case the polariton polarization dynamics is enriched the effects coming from the interference of forward and backward propagating polariton waves. To be able to describe these self-interference effects, we shell switch from the Stokes vector representation of the polariton intensity field to the Jones vector  $\mathbf{E} = (E_x, E_y)$  representation of the amplitude of this field, where  $E_{x,y}$  are the complex projections of the polariton field to  $x$ - and  $y$ -axes, respectively.  $\mathbf{E}$  and  $\mathbf{S}$  are linked between themselves by the following set of expressions (see Ref. [13, 20]):

$$S_0 = E_x E_x^* + E_y E_y^*, \quad (11a)$$

$$S_x = E_x E_x^* - E_y E_y^*, \quad (11b)$$

$$S_y = 2\Re(E_x E_y^*), \quad (11c)$$

$$S_z = 2\Im(E_x E_y^*). \quad (11d)$$

One can represent  $E_{x,y}$  in the following convenient form:

$$\mathbf{E} = \begin{pmatrix} \varepsilon_x e^{i(\omega t - \mathbf{k}\mathbf{r} + \phi_x)} \\ \varepsilon_y e^{i(\omega t - \mathbf{k}\mathbf{r} + \phi_y)} \end{pmatrix}, \quad (12)$$

where  $\varepsilon_{x,y} = |E_{x,y}|$  are the amplitudes of the field components,  $\omega$  and  $\mathbf{k}$  are a the frequency and the wave vector, respectively.  $\phi_{x,y}$  define phases of the polariton field components. We introduce an  $xy$  phase difference parameter  $\delta = \phi_y - \phi_x$  as well as the total phase which governs the oscillating term through the exponential factor  $i\omega t + i(\phi_x + \phi_y) \rightarrow i\omega t$ . As a result, with the foregoing redefinitions the Jones vector can be written as

$$\mathbf{E} = e^{i(\omega t - \mathbf{k}\mathbf{r})} \begin{pmatrix} E_x \\ E_y \end{pmatrix} = e^{i(\omega t - \mathbf{k}\mathbf{r})} \begin{pmatrix} \varepsilon_x e^{-\frac{i}{2}\delta} \\ \varepsilon_y e^{\frac{i}{2}\delta} \end{pmatrix}. \quad (13)$$

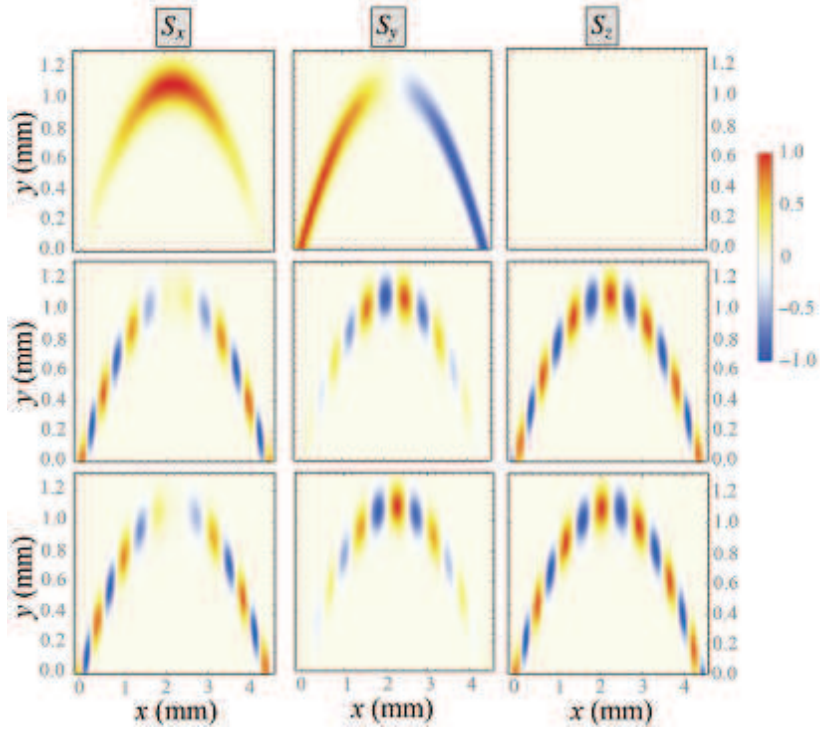


FIG. 9. (Color online) Polariton polarization components  $S_{x,y,z}$  of ballistically propagating exciton-polaritons. The initial polarization is taken diagonal linear with  $S_{y,0} = 1$  for the upper panels, linear with  $S_{x,0} = 1$  for the middle panels and circular with  $S_{z,0} = 1$  for the lower panels. The magnetic field  $B = 0$ , the initial wave number is taken  $k = 5500 \text{ mm}^{-1}$ , the shooting angle is taken  $45^\circ$  ( $k_x = k_{y,0} = k/\sqrt{2}$ ) for all the panels.

From (11)–(13) we find

$$\varepsilon_x = \sqrt{\frac{1}{2}(S_0 + S_x)}, \quad (14a)$$

$$\varepsilon_y = \sqrt{\frac{1}{2}(S_0 - S_x)}, \quad (14b)$$

$$\delta = \arctan_2[S_z/S_y], \quad (14c)$$

where  $\arctan_2(b/a) = -i \ln \left[ \frac{a+ib}{\sqrt{a^2+b^2}} \right]$ .

We formally split the ballistically propagating polariton wave into two waves, namely the forward wave  $\mathbf{E}^{(f)}$  (before the turning point) and the backward wave  $\mathbf{E}^{(b)}$  (after the turning point) denoting  $\mathbf{E}^{(f,b)} = (E_x^{(f,b)}, E_y^{(f,b)})^T$ . To calculate the resulting total field  $\mathbf{E}^{(f)} + \mathbf{E}^{(b)}$  we can formally replace  $t \rightarrow t_{\text{turn}} - t$  for  $\mathbf{E}^{(b)}$ .

Figure 8 shows the interference intensity pattern  $I_{\text{fb}} = |\mathbf{E}^{(f)} + \mathbf{E}^{(b)}|^2$  as a function of  $B$ . The picture is similar for all initial polarization states of the fully polarized polariton field. It is reminiscent of the interference of an incident and a reflected waves in the case of a conventional coherent reflection of light by a mirror. However, in contrast with the latter case, the phase of the backward wave changes continuously and does not show a discontinuity with the incident wave phase at the mirror surface. The interference picture has a complex structure in the presence of the magnetic field. At  $B \approx \pm 1.5 \text{ T}$  for the used parameters the picture is blurry. The origin of this effect has been considered in the previous subsection. The blurry picture correspond to the regime of a reduced  $|\dot{\mathbf{S}}|$  and the Stokes vector trajectory tending to an attractor (see Fig. 7).

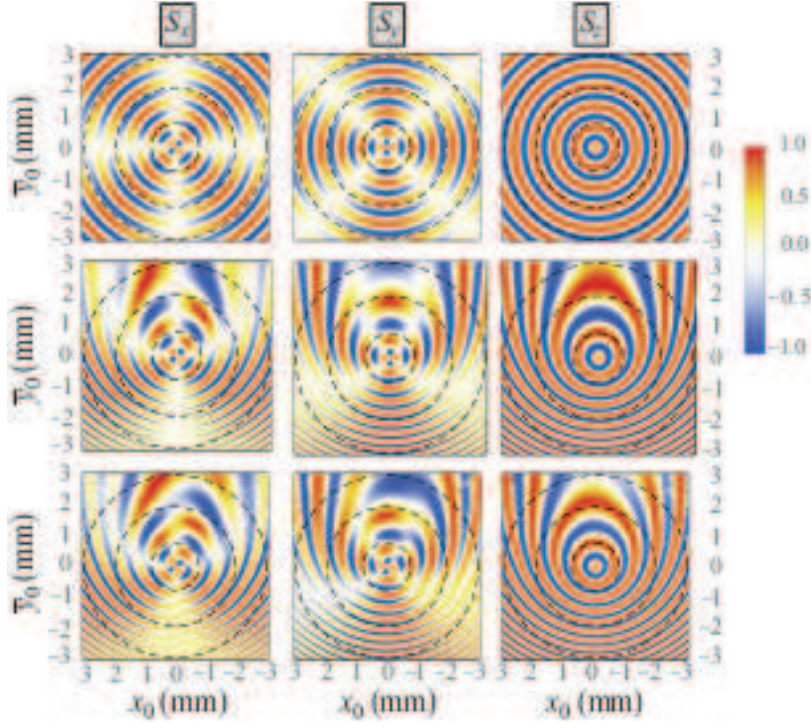


FIG. 10. (Color online) Polarization patterns resulting from the pulsed excitation of polaritons by a point-like source calculated at different values of  $\beta$  and  $B$ . For the upper panels,  $\beta = 0$ ,  $B = 0$ ; for the middle panels,  $\beta = 10.5$  meV/mm,  $B = 0$ ; for the lower panels,  $\beta = 10.5$  meV/mm,  $B = 2.5$  T. The initial polarization is taken circular with the initial conditions  $S_{x,y,0} = 0$ ,  $S_{z,0} = 1$ . For the clarity of representation, in the middle and lower panels we introduce a new dynamically shifted coordinate  $\bar{y}_0 = y_0 + \beta t^2 / 2m^*$ . Dashed circles (from the inner to the outer) correspond to  $t = 60$  ps,  $t = 150$  ps and  $t = 230$  ps.

#### IV. PROPAGATION OF POLARITONS IN THE OBLIQUE TO THE GRADIENT DIRECTION

##### A. Single Polariton Propagation

In practice, we have one more external control parameter in our problem that is the shooting angle  $\theta$ , the angle between the initial polariton wave vector and  $x$ -axis. In this case,  $k_x$  and the related parameter  $\Omega_y$  differ from zero and  $x_0$  also becomes time-dependent. The main difference from the case considered above is that now the particle propagates along a parabolic trajectory, hence the forward and the backward branches are separated by a distance  $\frac{2\hbar^2 k^2}{m^* \beta} \frac{|\tan[\theta]|}{1 + \tan^2[\theta]}$  in the  $x$  direction at the latitude  $x_0 = 0$ . In [7] the spatial separation between forward and backward going polaritons helped measuring the long-living polariton lifetime since it allowed eliminating the spurious radiation resulting from the reflection of the excitation laser.

Figure 9 demonstrates the spatial distribution of the polariton polarization components  $S_{x,y,z}$  in the cavity plane for different initial conditions in the absence of the external magnetic field,  $B = 0$ . The initial polarizations are taken  $S_{y,0} = 1$  for the upper panels,  $S_{x,0} = 1$  for the middle panels and  $S_{z,0} = 1$  for the lower panels. The other initial polarization components are taken equal to zero in all cases. The polarization components  $S_{x,y,z}$  are multiplied by the spatially dependent wave packet intensity of the polariton field. The incident wave packet is governed by the shape of the Gaussian form  $\Psi \sim \exp[-(y - y_0)^2 / 2y_w^2]$  with  $y_w = 0.1$  mm and the time-dependent “center of mass” coordinates  $(x_0(t), y_0(t))$ . The upper panels in Fig. 9 demonstrate the transformation of the diagonal linear polarization  $S_{y,0} = 1$  to the antidiagonal one,  $S_y = -1$ . The Stokes vector evolves from  $S_{y,0} = 1$  to  $S_y = -1$  passing by the  $S_x = 1$  state. The component  $S_z$  is close to zero in this case. The middle and the lower panels demonstrate the inversion of the linear (middle) and circular (lower) polarizations, as one can see comparing the polarization patterns before and after the turning point.

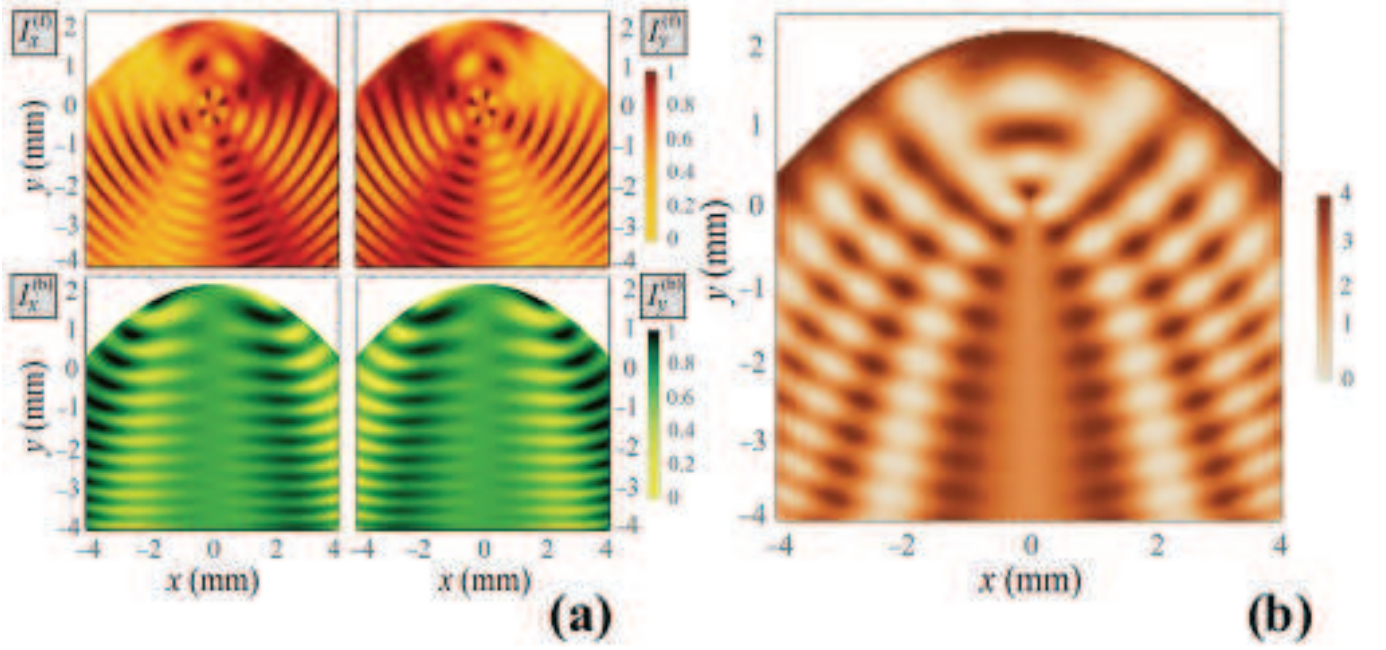


FIG. 11. (Color online) Upper panels in the left – intensity of the components of the forward propagating polariton field. Middle panels – intensity of the components of the backward propagating polariton field. Lower panel – patterns resulting from the self-interference of the polariton field emitted by a point source placed in  $(0,0)$  point. The magnetic field is taken  $B = 0$ .

### B. The Pulsed Excitation of Exciton-Polaritons by a Point-like Source

We now consider the polarization dynamics of the cylindrical polariton wave packet emitted by a point-like source with the coordinates  $(x_0(0), y_0(0)) = (0, 0)$ . The initial polarization of the polaritons is taken circular with  $S_{x,0} = S_{y,0} = 0$  and  $S_{z,0} = 1$ . Figures 10 represent the parametric dependencies of the polariton polarization components on the spatial coordinates:  $x_0$  and the shifted coordinate  $\bar{y}_0 = y_0 + \frac{\beta t^2}{2m^*}$ . The black dashed circles in Fig. 10 correspond to  $t = 60$  ps, 150 ps and 230 ps (counting from the inner to the outer circle).

The upper row panels illustrate the trivial case without the “gravitational” force ( $\beta = 0$ ) and the magnetic field ( $B = 0$ ). It is the case discussed in Ref. 14 and showing the signature of the optical spin Hall effect. In the middle row panels, the “gravitation” is switched on,  $\beta = 10.5$  meV/mm. In this case, the polarization patterns “fall down” in time and the symmetry (or anti-symmetry) of the patterns with respect to the point moving with the velocity  $-\beta t/m^*$  down the  $y$  direction is conserved. In the lower row panels, the magnetic field  $B = 2.5$  T has been added as well. The magnetic field  $B$  breaks the pattern symmetry and induces the rotation of the patterns clockwise for  $B < 0$  and anticlockwise for  $B > 0$ . Since we do not consider a continuous pump here, the interference effects are absent.

### C. Self-Interference of a Polariton Flow Excited by a Point-like Source in the CW Regime

In contrast with the previous subsection, here we consider the case where the point  $(0,0)$  is a source of continuous polariton waves. In this case, effects of interference take place. Similarly to the approach used in the subsection III B, here we decompose the polariton wave  $\mathbf{E}$  into the forward,  $\mathbf{E}^{(f)}(x_0, y_0)$ , and the backward,  $\mathbf{E}^{(b)}(x_0, y_0)$ , waves. The upper row in Fig. 11 represents the intensities of  $x$  and  $y$  components of the wave  $\mathbf{E}^{(f)}$ . It is clearly seen that it resembles a cylindrical wave. In  $+y$  direction the wave is limited by a “slow mirror” boundary that has a parabolic shape. This shape can be found analytically from Eqs. (4) calculated for two points. One point with the coordinates  $(0, y_1 = y_{\max})$  corresponds to the turning point for the propagation along the thickness gradient with  $k_x = 0$  and  $k_y = k$ . The other point,  $(x_2, 0)$ , belongs to the widest in  $x$ -direction trajectory with  $k_x = k_y = k/\sqrt{2}$ . The final expression for the shaft of the “slow mirror” is given by

$$y_m = \frac{\hbar^2 k^2}{2\beta m} - \frac{\beta m}{\hbar^2 k^2} x_m^2. \quad (15)$$

The backward wave  $\mathbf{E}^{(b)}$  appearing after the “slow reflection” is close to a plane wave, see the middle row in Fig. 11. The similarity becomes even stronger at the large time  $t$ . The lower panel in Fig. 11 demonstrates the self-interference pattern of the point-source polariton field. A similar effect is known for parabolic mirrors that “straighten” spherical waves to the plane waves. In our case, the parabolic “slow mirror” of exciton-polaritons is self-induced by a point-like polariton source placed in a wedged microcavity.

## V. CONCLUSIONS

We have considered the dynamics of exciton-polaritons propagating over large distances in wedged microcavities in the presence of the TE-TM splitting and external magnetic field. The cavity thickness gradient playing role of artificial gravity strongly affects the TE-TM splitting and the speed of propagating polaritons. We demonstrated theoretically the formation of polarization patterns in the real space due to the optical spin Hall effect and “slow reflection”.

We have demonstrated the possibility of manipulating the polariton polarization state by choosing the excitation laser incidence angle and the magnitude of the magnetic field. Interestingly at the specific combinations of the magnetic field and the initial polariton wave vector the polariton Stokes vector tends to an attractor on the surface of the Poincaré sphere.

The “gravitational” force compelling polaritons to change both magnitude and direction of their wave vector is the cause of another fascinating effect that is the self-interference of a spin-polarized polariton field. We show that for a point-like polariton source, the wedged microcavity acts analogous to a parabolic mirror performing “slow reflection” and transforming a cylindrical-like polariton wave to a counterpropagating plane-like wave. The interfering waves create peculiar intensity and polarization patterns. The effects discussed here may be used in future polariton spin transistors and logical gates.

## ACKNOWLEDGMENTS

This work was supported by the EPSRC Hybrid Polaritonics Programme grant. The work of E.S. was supported by the Russian Foundation for Basic Research Grants No. 16-32-60104, No. 15-59-30406, and by grant of President of Russian Federation for state support of young Russian scientists No. MK-8031.2016.2. E.S. acknowledges I. Yu. Chestnov for valuable advices and fruitful discussions.

- 
- [1] Kasprzak J, Richard M, Kundermann S, Baas A, Jeambrun P, Keeling J M J, Marchetti F M, Szymanśka M H, Andreé R, Staehli J L, Savona V, Littlewood P B, Deveaud B, and Dang L S 2006 *Nature* **443** 409–6
  - [2] Amo A, Pigeon S, Sanvitto D, Sala V G, Hivet R, Carusotto I, Pisanello F, Lemenager G, Houdre R, Giacobino E, Ciuti C, and Bramati A 2011 *Science* **332** 1167–4
  - [3] Keeling J and Berloff N G 2011 *Contemporary Physics* **52** 131–21
  - [4] Nelsen B, Liu H, Steger M, Snoke D W, Balili R, West K, and Pfeiffer L 2013 *Phys. Rev. X* **3** 041015–8
  - [5] Steger M, Liu G, Nelsen B, Gautham C, Snoke D W, Balili R, Pfeiffer L and West K 2013 *Phys. Rev. B* **88** 235314–11
  - [6] Sermage B, Malpuech G, Kavokin A V, and Thierry-Mieg V 2001 *Phys. Rev. B* **64** 081303(R)–4
  - [7] Steger M, Gautham C, Snoke D W, Pfeiffer L, and West K 2015 *Optica* **2** 1–5
  - [8] Gao T, Eldridge P S, Liew T C H, Tsintzos S I, Stavrinidis G, Deligeorgis G, Hatzopoulos Z, and Savvidis P G 2012 *Phys. Rev. B* **85** 235102–5
  - [9] Maialle M Z, de Andrada e Silva E A, and Sham L. J 1993 *Phys. Rev. B* **47** 15776–13
  - [10] Kavokin A 2012 Spin Effects in Exciton-Polariton Condensates *Exciton Polaritons in Microcavities. New Frontiers* ed Sanvitto D, Timofeev D (Berlin Heidelberg: Springer-Verlag) pp 233–244
  - [11] Panzarini G, Andreani L C, Armitage A, Baxter D, Skolnick M S, Astratov V N, Roberts J S, Kavokin A V, Vladimirova M R, and Kaliteevski M A 1999 *Phys. Rev. B* **59** 5082–8
  - [12] Shelykh I A, Rubo Yu G, and Kavokin A V 2007 *Superlattices and Microstructures* **41** 313–8
  - [13] Kavokin A, Baumberg J J, Malpuech G, and Laussy F P 2007 *Microcavities* (Oxford University Press)
  - [14] Kammann E, Liew T C H, Ohadi H, Cilibrizzi P, Tsotsis P, Hatzopoulos Z, Savvidis P G, Kavokin A V, and Lagoudakis P G 2012 *Phys. Rev. Lett.* **109** 036404–5
  - [15] Kavokin K V, Shelykh I A, Kavokin A V, Malpuech G, and Bigenwald P 2004 *Phys. Rev. Lett.* **92** 017401–4
  - [16] Gippius N A, Shelykh I A, Solnyshkov D D, Gavrilov S S, Rubo Y G, Kavokin A V, Tikhodeev S G, and Malpuech G 2007 *Phys. Rev. Lett.* **98** 236401–4
  - [17] Amo A, Liew T C H, Adrados C, Houdré R, Giacobino E, Kavokin A V, and Bramati A 2010 *Nat. Photonics* **4** 361–6



- [18] Kochereshko V P, Durnev M V, Besombes L, Mariette H, Sapega V F, Askitopoulos A, Savenko I G, Liew T C H, Shelykh I A, Platonov A V, Tsintzos S I, Hatzopoulos Z, Savvidis P G, Kalevich V K, Afanasiev M M, Lukoshkin V A, Schneider C, Amthor M, Metzger C, Kamp M, Höfling S, Lagoudakis P, and Kavokin A 2016 *Sci. Rep.* **6** 20091–6
- [19] Solnyshkov D D, Glazov M M, Shelykh I A, Kavokin A V, Ivchenko E L, and Malpuech G 2008 *Phys. Rev. B* **78** 165323–8
- [20] Theocaris P E, and Gdoutos E 1979 *Matrix Theory of Photoelasticity* (Springer-Verlag: New York)